

Retraction

Retracted: Diagnosis of Bronchial and Pulmonary Fungal Infection Using Gradient Weighted Denoising Algorithm-Based CT Images

Scientific Programming

Received 17 October 2023; Accepted 17 October 2023; Published 18 October 2023

Copyright © 2023 Scientific Programming. This is an open access article distributed under the Creative Commons Attribution License, which permits unrestricted use, distribution, and reproduction in any medium, provided the original work is properly cited.

This article has been retracted by Hindawi following an investigation undertaken by the publisher [1]. This investigation has uncovered evidence of one or more of the following indicators of systematic manipulation of the publication process:

- (1) Discrepancies in scope
- (2) Discrepancies in the description of the research reported
- (3) Discrepancies between the availability of data and the research described
- (4) Inappropriate citations
- (5) Incoherent, meaningless and/or irrelevant content included in the article
- (6) Peer-review manipulation

The presence of these indicators undermines our confidence in the integrity of the article's content and we cannot, therefore, vouch for its reliability. Please note that this notice is intended solely to alert readers that the content of this article is unreliable. We have not investigated whether authors were aware of or involved in the systematic manipulation of the publication process.

Wiley and Hindawi regrets that the usual quality checks did not identify these issues before publication and have since put additional measures in place to safeguard research integrity.

We wish to credit our own Research Integrity and Research Publishing teams and anonymous and named external researchers and research integrity experts for contributing to this investigation.

The corresponding author, as the representative of all authors, has been given the opportunity to register their agreement or disagreement to this retraction. We have kept a record of any response received.

References

- [1] H. Hu, L. Zhou, and P. Zhang, "Diagnosis of Bronchial and Pulmonary Fungal Infection Using Gradient Weighted Denoising Algorithm-Based CT Images," *Scientific Programming*, vol. 2022, Article ID 4716572, 8 pages, 2022.

Research Article

Diagnosis of Bronchial and Pulmonary Fungal Infection Using Gradient Weighted Denoising Algorithm-Based CT Images

Hao Hu , Lihua Zhou , and Peng Zhang 

Department of Radiology, Wuhan Fourth Hospital, Puai Hospital, Tongji Medical College, Huazhong University of Science and Technology, Wuhan 430033, Hubei, China

Correspondence should be addressed to Peng Zhang; 20162103821@mails.imnu.edu.cn

Received 30 August 2021; Revised 11 January 2022; Accepted 18 January 2022; Published 10 February 2022

Academic Editor: Gustavo Ramirez

Copyright © 2022 Hao Hu et al. This is an open access article distributed under the Creative Commons Attribution License, which permits unrestricted use, distribution, and reproduction in any medium, provided the original work is properly cited.

Based on computed tomography (CT) with a gradient weighted denoising algorithm, the image denoising technique was applied to diagnose bronchial and pulmonary fungal infection to discuss the features of CT images and the efficiency of the denoising algorithm. Therefore, it could assist clinicians in disease treatment. The clinical data and imaging data of 100 patients with invasive pulmonary fungal infection were collected in the hospital. All of them were rolled into a natural denoising CT group (routine group) and gradient weighted denoising algorithm-based image denoising group (algorithm group). The images from the routine group were processed by the routine natural denoising method, and the images from the algorithm group were denoised with the gradient weighted denoising algorithm. The results showed that the algorithm group had greater denoising efficiency and less denoising time compared with the routine group ($P < 0.05$). The diagnostic sensitivity, specificity, and accuracy of the denoised images from the algorithm group were higher markedly than the above three indicators of the routine group ($P < 0.05$). For bronchopulmonary infections, the sensitivity, specificity, and accuracy of the PDE model for CT denoised images were 99.00%, 96.87%, and 98.33%, the positive rate of chest CT examination was 86.2%, which was higher markedly than the rate of ordinary CT examination (70.5%), and the difference was statistically substantial ($P < 0.05$). Besides, the mean absolute error (MAE), peak signal to noise ratio (PSNR), and mean structural similarity index measure (MSSIM) of the algorithm group were better than those of the unprocessed images and the routine group ($P < 0.05$). Moreover, the algorithm group had a good visual effect. In conclusion, the gradient weighted denoising algorithm could effectively remove the noise and bar artifacts in CT images and well retain the edge details of CT images, thereby improving the quality of CT images. Therefore, it was suitable for clinical diagnosis and had practical application value.

1. Introduction

The incidence of invasive pulmonary fungal infection (IPFI) has been increasing year by year and has become the focus of research in recent years [1–3]. The early detection and diagnosis of pulmonary fungal disease, especially IPFI, is the key to the treatment of pulmonary fungal disease. In order to quickly, reliably, safely, and conveniently find a method for the diagnosis of pulmonary fungi, early detection, timely treatment, and reduction of mortality, it is of great practical value and significance [4].

With the development of imaging science, especially the continuous innovation of X-ray computed tomography (CT) imaging technology, the microstructure and the subtle

pathological changes of the lung can be fully displayed. The use of imaging to detect and diagnose pulmonary fungal infections is a critical research topic in this field [5]. The 2006 Diagnostic Criteria and Treatment Principles for Invasive Pulmonary Fungal Infections (Draft) listed the characteristic imaging manifestations of pulmonary aspergillus infectious disease and fungal pneumonia as the main clinical indicators of the diagnostic criteria, but other findings of the characteristic images have not been defined yet [6]. Therefore, this study conducted a comprehensive study and discussion on the features and evolutionary rules of image observation through the retrospective analysis of clinical observation.

Under the trend of economic globalization, the rapid development of computer technology and artificial

intelligence (AI) technology has prompted humans to expand their visual functions through digital image processing to visualize physical images [7]. In addition to the use of CT magnetic resonance imaging, the overall performance of digital image processing systems for clinical diagnosis depends on the quality of the measured images. However, digital images are collected, and they are inevitably contaminated by noise during the compression, transmission, and storage processes [8]. At present, the application of CT postprocessing in medical image processing is the main research hotspot in the field of image noise removal [9].

In the field of image processing and computer vision, the image denoising method based on the gradient weighted denoising algorithm has the advantages of relatively complete theoretical support and flexible numerical format [10, 11]. In the last 20 years, the field of image denoising has developed its own scope. The difficulty of statistical modeling of unequal speckle noise and stripe artifacts in medical CT images is considered, so the image noise removal method based on gradient weighting is a fine noise removal method that processes each pixel in the image [12]. At present, most image noise elimination models and algorithms can remove the added white Gaussian noise in natural images, but they cannot effectively eliminate speckle noise and artifacts in CT images. In this study, an image denoising method based on gradient weighting was investigated, and a denoising method suitable for natural images was designed. This method had edge preservation and good noise reduction performance, which also had practical value in the field of image preprocessing. The new method could effectively suppress noise and streak artifacts in CT postprocessing and maintain the structural features of clinical diagnosis, which was a valuable asset for the research and development of human health system engineering. In a word, the research of the image denoising method based on gradient weighting had vital theoretical importance and good application prospects.

In this study, an image denoising method based on a gradient weighted denoising algorithm was employed to reduce bronchial infection, and the medical CT images were observed; the values of mean absolute error (MAE), peak signal to noise ratio (PSNR), and mean structural similarity index measure (MSSIM) were measured to judge the denoising efficiency.

2. Methods

2.1. Research Objects. There was a collection of the clinical data and imaging data of patients diagnosed or clinically diagnosed with an invasive pulmonary fungal infection from April 2016 to April 2020 in the hospital.

The inclusion and exclusion criteria are as follows.

Inclusion criteria: (1) positive histochemical or cytochemical tests for mycelia or particles (nonyeast), lung tissue specimens, pleural fluid, and blood cultures. (2) Yeast cells and/or pseudomyelia were detected by histochemical or cytochemical methods in lung tissue samples. Yeast cultures in lung tissue specimens, pleural effusion, or blood are positive, and microscopic examination shows fungal

infection. Exclusion criteria: pneumococcal pneumonia, bronchopulmonary mycosis caused by fungal parasitism and allergy, concurrent infection with other pathogens (bacteria, mycoplasma, virus, tuberculosis, etc.), and no lung CT data.

In this study, a total of 100 patients with bronchial fungal infections were selected, who met the above inclusion criteria and exclusion criteria. This study was approved by the Medical Ethics Committee of the hospital, and the family members of the patients included in the study signed an informed consent form.

2.2. CT Examination Methods. The chest CT scanning was carried out through Toshiba 16-row CT and Philips 64-row CT. The thickness of the reconstruction layer was 7 mm or 5 mm; CT scanning was enhanced; 70–90 mL of nonionic contrast agent was used for intravenous injection, and the injection speed was 5 mL/s. Scanning was performed in 3–5 minutes after 30–52 seconds of injection.

2.3. Gradient Weighted Denoising Algorithm

2.3.1. Gradient Weighted Partial Differential Equation Model. The representative methods of denoising based on transformed regions include Fourier transform, wavelet transform, principal component analysis, principal component analysis (PCA), and sparse representation. These transformation region image denoising methods have become hot spots in the research of transform region denoising methods [13]. However, the nontranslation invariant wavelet transform method is easy to produce a pseudo Gibbs effect near the discontinuity of the denoising image. A weighted curvature-preserving partial differential equation (WCPDE) diffusion model was proposed in this study. The central theory of these models is to adjust the diffusion behaviour of the model by using the edge indicator and the local geometric features of the image defined in the edge direction. What is more, the diffusion matrix replaces the scalar diffusion coefficient. This model provides greater flexibility for processing directed structural information on a point-to-point basis. The PDE model is specifically defined as

$$\frac{x^u}{x^f} = di \ v(D\nabla u), u_{i=0} = u_0. \quad (1)$$

In the above equation, u stands for the image intensity function; u_0 means a given image; ∇ indicates a gradient operator; and D represents a diffusion tensor. The eigenvalue of the diffusion tensor D controls the intensity of the diffusion during the diffusion process, and the specific definition is as follows:

$$D = \left\{ C1 = \max\left(0.01, 1 - e^{-(r_1 - r_2)^{2/x}}\right), C2 = 0, 01 \right\}. \quad (2)$$

In the above equation, r expresses a very small constant parameter, which was set to $r = 0.001$.

The numerical iterative algorithm of the PDE model can be summarized as the following flowchart shown in Figure 1.

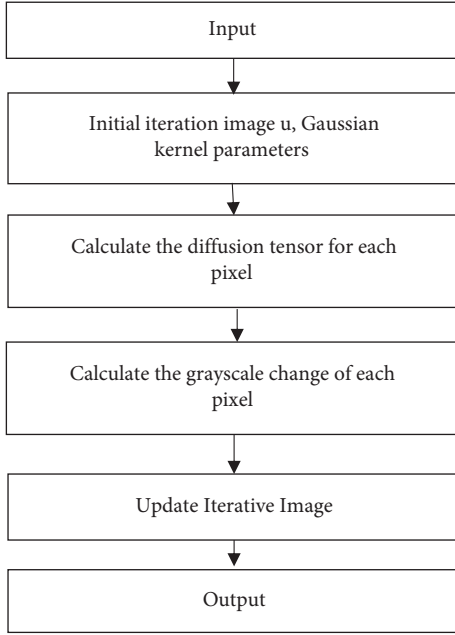


FIGURE 1: Iterative algorithm processing image flowchart.

2.4. Image Quality Evaluation Standard. In the field of image denoising, the denoising quality of images is analysed and evaluated for the evaluation of the image denoising methods. Since the uniform standard for image quality evaluation has not been formed, it is a problem that should be solved in the research of image processing to establish a set of image quality evaluation systems for integrity image processing. There are two types of image quality evaluation methods: subjective evaluation and objective evaluation.

Subjective evaluation methods are mainly based on visual effect evaluation and analysis of denoising images. Subjective evaluation is generally divided into three situations. One is to randomly select a group of observers in the observation environment and evaluate the image for two groups of subjective evaluation; the mean opinion score (MOS) is adopted to comprehensively evaluate the subjective quality of the image. The subjective evaluation method will spend much time in the whole process of evaluation. Real-time subjective image quality evaluation is not a practical method to use the knowledge of fuzzy mathematics theory to carry out an approximate quantitative evaluation of image quality, such as mean indicator method, method noise point, and the image indicator method. In some methods, the evaluation parameters need to be set manually. Based on the subjective observation of human judgment, the difference of image structure information between the image and the original image or noise image is removed by observation and comparison of noise. The objective evaluation method of denoising image quality is mainly based on the mathematical model of objectively calculating image quality. Current evaluation indicators mainly include MAE, PSNR, and MSSIM [14]. Furthermore, the denoising ability of the denoising algorithm can be judged by MAE and PSNR. The specific definition is as follows:

$$\text{MAE} = \frac{\sum_{w=1}^M \sum_{e=1}^N |u(w, e) - f(w, e)|}{M \times N}. \quad (3)$$

$$\text{PSNR} = 10 \log_{10} \left(\frac{255^2 \times M \times N}{\sum_{w=1}^M \sum_{e=1}^N |u(w, e) - f(w, e)|^2} \right). \quad (4)$$

In (3) and (4), $M \times N$ represents the size of CT; u and f are the original image and the noise-removed image, respectively. The higher the PSNR value, the smaller the MAE and the better the image denoising effect. The difference between the specified image and the original image is measured by the MSSIM standard from the three aspects of brightness, contrast, and structural information, and the performance of the denoising algorithm is also detected for preserving the edge details of the image. The specific definition is as follows:

$$\text{MSSIM}(u, f) = \frac{1}{N} \sum_{w=1}^N \text{SSIM}(x_w, y_w), \quad (5)$$

$$\text{SSIM}(x, y) = \frac{(2\alpha_x \alpha_y + c_1)(2\sigma_{xy} + c_2)}{(\alpha_x \alpha_y + c_1)(\sigma_x^2 + \sigma_y^2 + c_2)}. \quad (6)$$

In (5) and (6), u and f stand for the original image and the noise-removed image in turn; x and y represent the original image and the noise; N indicates the mean value of the grey value of the pixel, that is, the dispersion of the gray value of the pixel of the image. The c_1 and c_2 as the covariances of the graph blocks x and y are the small constants to make sure that the denominator is not zero. The larger the MSIIM value, the more similar the structural information between the noise-removed image and the original image.

The experiment is simulated in the environment of MATLAB 2016, I7-4770K CPU, 35 GHz, and Windows 7. The simulation experiment objectively evaluates the advantages and disadvantages of each denoising method. The comprehensive evaluation research is employed to determine the evaluation indicator of denoising effect, and the objective evaluation indicator of SNR is used to evaluate the quality of the evaluation area. The specific definition of SNR is as follows:

$$\text{SNR}(Q) = \frac{SI(Q)}{S D(Q)}. \quad (7)$$

In the above equation, I indicates the selected region of interest; D means the mean value of the pixel grey value of the region of interest; Q stands for the standard deviation of the pixel grey value of the region of interest.

2.5. Observation Indicators. Histological or sterile body fluid tests were used as the results of clinical comprehensive diagnosis, and the results of lung tissue biopsy were positive, or the results of sputum bacterial culture for the same fungus were positive for three consecutive times. The sensitivity, specificity, and accuracy of CT for the diagnosis of pulmonary fungal infections were calculated and compared.

Sensitivity = number of true positive cases / (true positive + false negative) cases \times 100%

Specificity = number of true negative cases / (true negative + false positive) cases \times 100%

Accuracy = (true positive + true negative) cases / total cases \times 100%

2.6. Statistical Methods. The data were statistically analysed with SPSS20.0 software. The absolute number was expressed as the mean \pm standard deviation, the relative number was expressed as the rate and ratio, and the comparison between groups was analysed by the exact probability method.

3. Results

3.1. Visual Comparison of Image Denoising Efficiency between Natural Denoising and Gradient Weighted Denoising Algorithm. In the simulation experiment of natural images, the head, chest, and buttocks images were denoised. In order to obtain the noise images, the mean value 0 and Gaussian noise 0.002 were added to the test images, respectively, and the denoising experiment was carried out on the noise images. For the denoising ability of the PDE model, subjective visual evaluation and objective evaluation indicators (MAE, PSNR, and MSSIM) were applied to evaluate and analyse the image quality of denoising. The parameters of each comparison model in the experiment were set based on the best experimental results. The subjective visual effects are shown in Figure 2, and Figure 3 shows the comparison results of objective evaluation performance indicators.

In the normal denoising process, the edge information of the image was well preserved, but the resulting noise had a poor visual effect, as shown in Figure 2. The processing result of the PDE model had a good visual effect, the image noise was effectively suppressed, the edge details were maintained well, and some weak edges and texture information in the image were eliminated. Thus, the visual effect became better, and the accuracy of the edge of the graph was maintained good.

From the objective evaluation standards in Figure 3, it was found that under the same noise state, the MAE, PSNR, and MSSIM obtained by the PDE model were all better than those of the unprocessed image and natural denoising. Therefore, PDE denoising had stronger denoising and edge detail protection capabilities.

3.2. CT Images of the Lungs with Fungal Infections. To verify the high-definition processing of medical CT images by the proposed PDE model and to verify its value in clinical applications, the chest cavity model and clinical data of actual CT scans were selected as experimental objects. The use ratio of each image was 1 : 1, and its size was to obtain the PDE algorithm to reconstruct the image, which further improved the quality of the reconstructed image.

Artifacts near natural denoising were stored as structural information, which could not meet the needs of clinical diagnosis. The result of natural denoising processing

preserved the edge information well, but it lost a lot of blood vessel details, which could not meet the needs of clinical diagnosis. The PDE algorithm had obvious effect advantages on the artifacts and edge preservation of CT images; the processing results were more refined and clearer, and it had more ideal visual effects to bring convenience to clinical diagnosis (Figure 4).

Using PSNR value, MSSIM value, and denoising time as objective performance evaluation indicators, the denoising performance in the actual lung CT image was measured. As shown in Figure 5, the PSNR value and MSSIM value were high, and the time was slightly longer, while the denoising PDE algorithm was better than other denoising methods in the quantitative evaluation of clinical data processing results, thereby further illustrating the effectiveness of the PDE algorithm in processing clinical data.

3.3. The Diagnostic Sensitivity, Specificity, and Accuracy of Routine CT and PDE Model CT Denoised Images for the Diagnosis of Bronchopulmonary Infection. According to the comprehensive clinical diagnosis results and data calculation, the sensitivity, specificity, and accuracy of routine CT for the diagnosis of bronchopulmonary infection were 95.33%, 89.12%, and 93.99%, respectively. For bronchopulmonary infections, the sensitivity, specificity, and accuracy of the PDE model for CT denoised images were 99.00%, 96.87%, and 98.33% in turn (Figure 6).

3.4. Comparison on the Positive Rate of Normal Chest CT in Patients with Lung Fungal Infections and CT Image Processing Based on Gradient Weighted Denoising Algorithm. The comparison of the two methods indicated that the positive rate of chest CT examination was 86.2%, which was higher markedly than the rate of ordinary CT examination (70.5%), and the difference was statistically substantial ($P < 0.05$), as shown in Figure 7.

3.5. The Pathological Features of Bronchial Infection Checked through Two Ways. Compared with the routine CT group, the pathological features of bronchial infection such as deep lobes, bronchial inflation sign, long burr sign, adjacent pleural thickening, lymphadenopathy, calcification, and other manifestations were obviously increased ($P < 0.05$), as shown in Figure 8.

3.6. Variable Analysis of Pulmonary Fungal Infections in Patients with Bronchiectasis. The variable analysis of pulmonary fungal infection in patients with bronchiectasis is shown in Figure 9. The main risk factors of pulmonary fungal infection in patients with bronchiectasis are age, underlying pulmonary diseases, diabetes, hypoproteinemia, antibiotic use, respiratory failure, and the use of glucosides. This study indicated that 70% of the patients with fungal infection were over 60 years old, and 62% of the patients were with fungal infection and underlying pulmonary diseases. The proportion of patients with diabetes was 58%. The proportion of patients with pulmonary fungal infection with

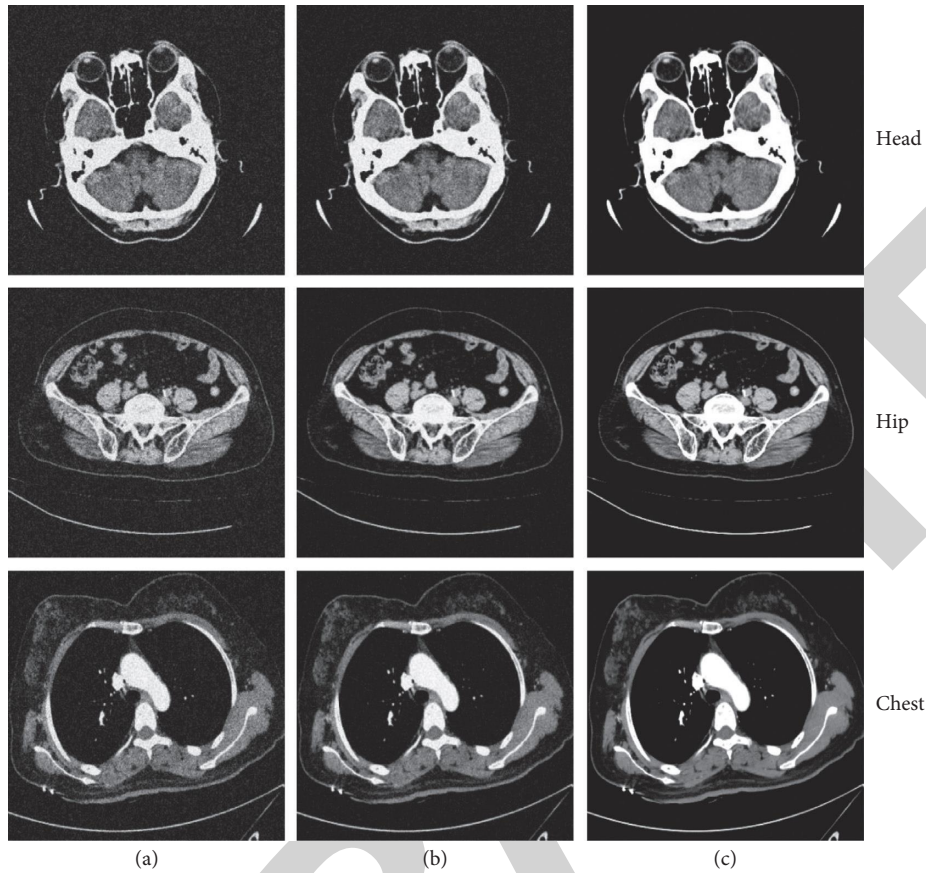


FIGURE 2: Visual comparison diagram after different methods of denoising processing of 38 years old. (a) Original image of CT image; (b) routine CT denoised image; (c) gradient weighted denoising algorithm-based CT denoised image.

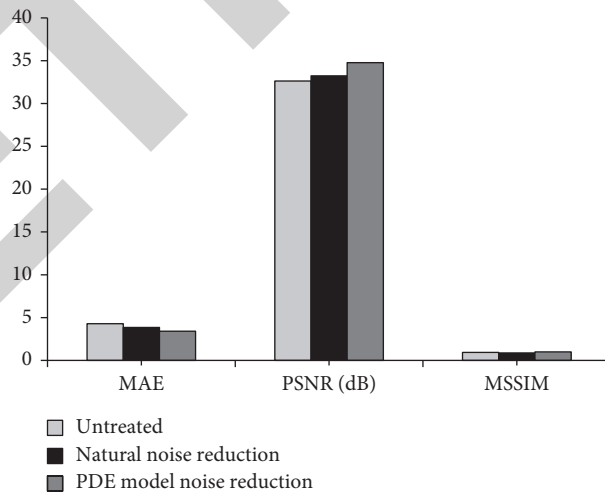


FIGURE 3: Comparison of objective evaluation performance indicators corresponding to unprocessed, natural denoising, and PDE denoising.

hypoproteinemia was 49%. Patients with pulmonary fungal infections who used glucoside accounted for 45%. Age, underlying pulmonary diseases, and diabetes are the main factors affecting pulmonary fungal infections. The elderly are more likely to develop pulmonary fungal infections;

underlying lung diseases can lead to lung environment disorders and bronchial epithelial cell damage, and fungi will invade the bronchial mucosa, deteriorating the state of bronchiectasis. Patients with diabetes also have an increased chance of developing pulmonary fungal infections.

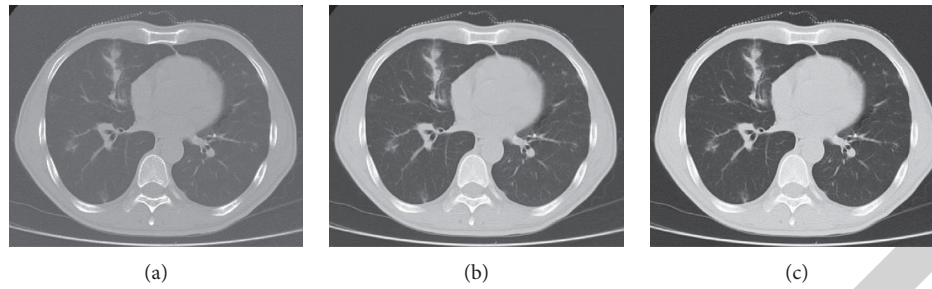


FIGURE 4: Visual comparison diagram after different methods of denoising processing of 46 years old. (a) Original image of chest CT image; (b) routine chest CT denoised image; (c) PDE algorithm-based chest CT denoised image.

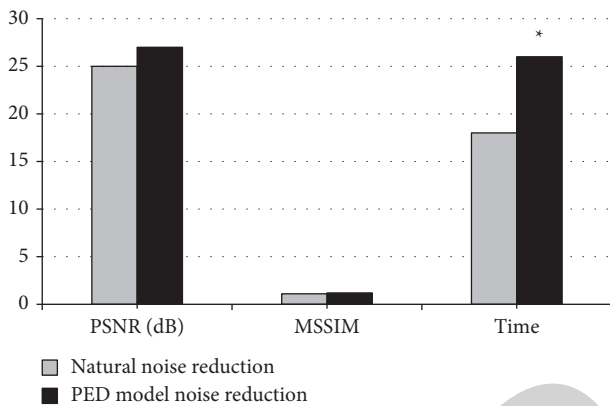


FIGURE 5: Comparison of PSNR value, MSSIM value, and denoising time between natural denoising and PDE algorithm. (* indicates difference between groups was statistically significant, $P < 0.05$).

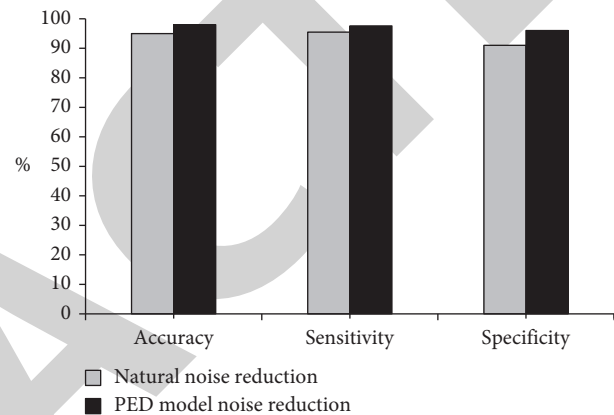


FIGURE 6: Comparison of the diagnostic sensitivity, specificity, and accuracy of routine CT and PDE model CT denoised images for the diagnosis of bronchopulmonary infection.

4. Discussion

Fungi are widely found in nature, most of which are opportunistic pathogens. In groups with immune function, the probability of fungal infection is very low, but fungi are harmful to the human body and have a serious impact on the life safety of patients. Among them, the highest rate of human fungal infection is found in the respiratory apparatus system [13]. In recent years, with the extension of human life expectancy and the wide application of hormones, broad-spectrum antimicrobial drugs, and immunosuppressive agents, the incidence of fungal infection has increased rapidly [15]. Fever, cough, sputum, hemoptysis, and dyspnea are the common symptoms of patients with pulmonary mycopathology. The key to the mortality of patients with fungal infection lies in the early diagnosis and rapid treatment of the results. The latest clinical diagnostic standard of fungal infection is etiological examination, long culture time, and susceptibility to contamination with a false positive; rapid and effective diagnosis is of great significance to improve the prognosis of patients with pulmonary mycosis if it is prolonged and easily contaminated with false positive [14]. In recent years, image examination has been carried out in the diagnosis of pulmonary mycosis, especially the development of CT technology, which plays a role in this technology. This technology has a very high resolution and can detect the microscopic pathological changes of the lung. Compared with ordinary CT images with natural denoising, the CT

examination has more advantages in disease display and clinical application value. CT findings of mycosis are complex and varied, with physiological features such as deep lobulation, air bronchial sign, long burr sign, adjacent pleural thickening, lymph node enlargement, and calcification [16]. The PDE algorithm takes into account the advantages of the first-order variational model and the second-order variational model. According to the gradient modulus of the image and the local fusion feature detection factor, the image is divided into flat areas and detailed areas. The variational order is selected adaptively in different regions to realize different diffusion modes. At the same time, the split PDE algorithm based on the fast Fourier transform (FFT) is used to solve the proposed variational model, which promotes the computing speed [17]. Under the guidance of the function, the image based on the gradient weighted denoising algorithm has larger smoothness in the flat region of the image and smaller smoothness in the edge region. Compared with other images, the edge region of the image and its characteristics are better preserved.

In this study, the experimental results disclosed that the proposed model had good visual effects for natural image denoising, as well as better MAE, PSNR, and MSSIM. It could effectively remove the noise and strip artifacts in the CT image and preserve the edge details of the image. Therefore, it could greatly improve the quality of the CT image, which was suitable for clinical diagnosis and had practical application value.

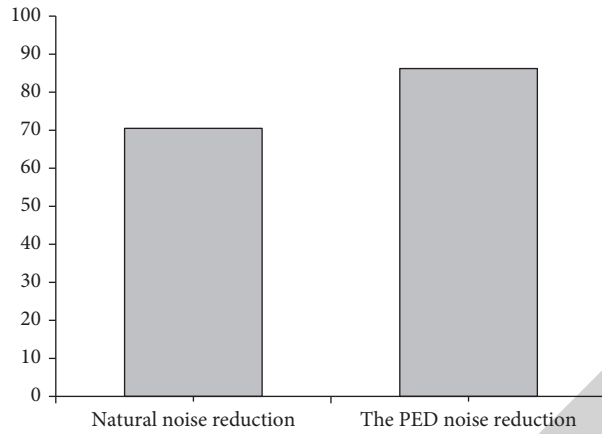


FIGURE 7: Comparison of the positive rates of the two methods.

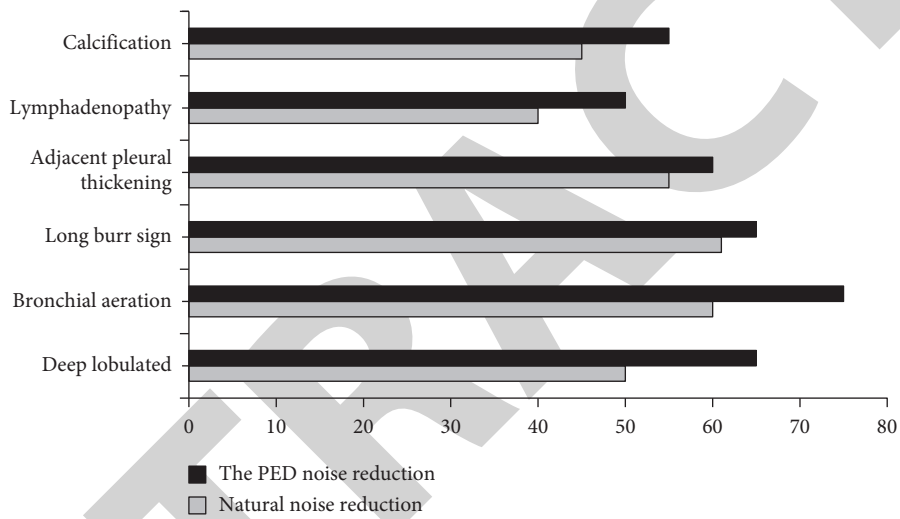


FIGURE 8: The detection rates of deep lobes, bronchial inflation sign, long burr sign, adjacent pleura thickening, lymph node enlargement, and calcification in two kinds of CT images.

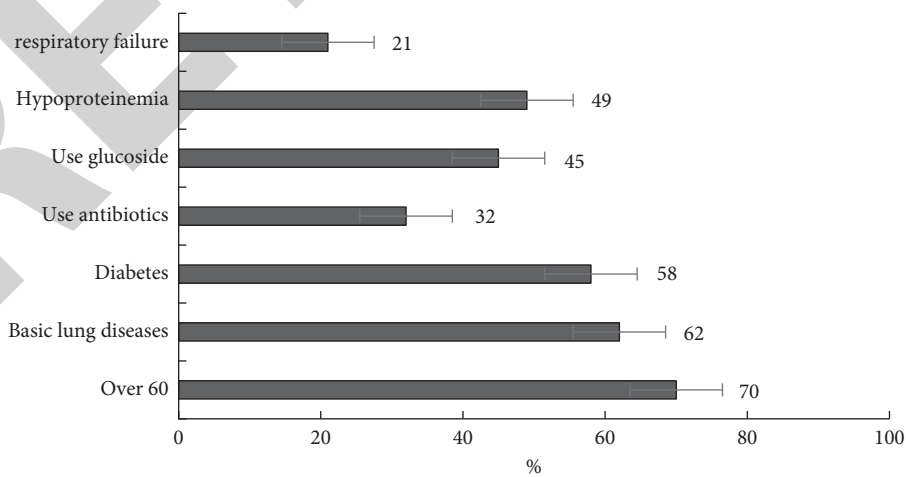


FIGURE 9: Variable analysis of pulmonary fungal infection in patients with bronchial infection.

5. Conclusion

The results of this study showed that CT images based on gradient weighted denoising algorithms were applied in the diagnosis and treatment of bronchopulmonary fungal infections. Compared with the routine CT denoising method, the processing results of the PDE model had better vision under the same noise conditions. As a result, image noise was effectively suppressed, edge details were well preserved, and some weak edges and texture information in the image were smoothed, with better visual effects, so that the edge details of the image were well maintained. The MAE, PSNR, and MSSIM obtained by the PDE model were all superior to the unprocessed images and natural denoising, and its diagnostic sensitivity, specificity, and accuracy were also higher than those of routine CT. However, this study also has the shortcomings of a small sample size, which needs to be further expanded. This lays the foundation for improving the clinical diagnosis rate of the disease, reducing the misdiagnosis rate and missed diagnosis rate, and improving the therapeutic effect. [18, 19].

Data Availability

The data used to support the findings of this study are available from the corresponding author upon request.

Conflicts of Interest

The authors declare no conflicts of interest.

Authors' Contributions

Hao Hu and Lihau Zhou contributed equally to this work.

References

- [1] M. Á. Martínez-García, L. Máiz, C. Oliveira et al., "Normativa sobre el tratamiento de las bronquiectasias en el adulto," *Archivos de Bronconeumología*, vol. 54, no. 2, pp. 88–98, 2018 Feb, English, Spanish.
- [2] F. Mbaye, "Maladie des moules bronchiques compliquée de pleurésie purulente : à propos d'un cas," *Revue des Maladies Respiratoires*, vol. 36, no. 1, pp. 63–68, 2019 Jan, French.
- [3] F. Z. Zhang, L. Qin, J. X. Yuan, and L. F. Tang, "Plastic bronchitis due to adenoviral infection: a case report," *BMC Pediatrics*, vol. 20, no. 1, p. 61, 2020 Feb 10.
- [4] L. Liang, L. Jin, and Y. Xu, "PDE learning of filtering and propagation for task-aware facial intrinsic image analysis," *IEEE Transactions on Cybernetics*, vol. 19, pp. 1–14, 2020 May 27.
- [5] L. Burzawa, L. Li, X. Wang, A. Buganza-Tepole, and D. M. Umulis, "Acceleration of PDE-based biological simulation through the development of neural network meta-models," *Current Pathobiology Reports*, vol. 8, no. 4, pp. 121–131, 2020 Dec.
- [6] E. Lovsin Barle, T. Pfister, C. Fux, D. Röthlisberger, D. Jere, and H.-C. Mahler, "Use of the permitted daily exposure (PDE) concept for contaminants of intravitreal (IVT) drugs in multipurpose manufacturing facilities," *Regulatory Toxicology and Pharmacology*, vol. 101, pp. 29–34, 2019 Feb.
- [7] Y. Li and L. Xia, "Coronavirus Disease 2019 (COVID-19): role of chest CT in diagnosis and management," *American Journal of Roentgenology*, vol. 214, no. 6, pp. 1280–1286, 2020 Jun.
- [8] N. Tzoumas, T. E. Farrah, N. Dhaun, and D. J. Webb, "Established and emerging therapeutic uses of PDE type 5 inhibitors in cardiovascular disease," *British Journal of Pharmacology*, vol. 177, no. 24, pp. 5467–5488, 2020 Dec.
- [9] Z. Ridha, L. Ouchene, E. Netchiporouk, and M. J. Gooderham, "Topical PDE-4 inhibitors are emerging for psoriasis treatment," *Journal of Cutaneous Medicine and Surgery*, vol. 25, no. 1, pp. 109–110, 2021 Jan-Feb.
- [10] K. Wójcik-Pszczola, G. Chłoń-Rzepa, A. Jankowska et al., "A novel, pan-PDE inhibitor exerts anti-fibrotic effects in human lung fibroblasts via inhibition of TGF- β signaling and activation of cAMP/PKA signaling," *International Journal of Molecular Sciences*, vol. 21, no. 11, p. 4008, 2020 Jun 3.
- [11] Z. Lv, X. Li, and W. Li, "Virtual reality geographical interactive scene semantics research for immersive geography learning," *Neurocomputing*, vol. 254, pp. 71–78, 2017.
- [12] E. Lejeune and B. Zhao, "Exploring the potential of transfer learning for metamodels of heterogeneous material deformation," *Journal of the Mechanical Behavior of Biomedical Materials*, vol. 117, p. 104276, 2021 May.
- [13] Y. Liao, X. Li, T. Mou et al., "Distinct infection process of SARS-CoV-2 in human bronchial epithelial cell lines," *Journal of Medical Virology*, vol. 92, no. 11, pp. 2830–2838, 2020 Nov.
- [14] J. Zhu, P. Mallia, J. Footitt et al., "Bronchial mucosal inflammation and illness severity in response to experimental rhinovirus infection in COPD," *The Journal of Allergy and Clinical Immunology*, vol. 146, no. 4, pp. 840–850, 2020 Oct, e7.
- [15] J. L. Lopez-Campos, M. Miravittles, D. de la Rosa Carrillo, R. Cantón, J. J. Soler-Cataluña, and M. A. Martínez-García, "Current challenges in chronic bronchial infection in patients with chronic obstructive pulmonary disease," *Journal of Clinical Medicine*, vol. 9, no. 6, p. 1639, 2020 May 28.
- [16] A. Valipour, S. Fernandez-Bussy, A. J. Ing et al., "Bronchial rheoplasty for treatment of chronic bronchitis. Twelve-month results from a multicenter clinical trial," *American Journal of Respiratory and Critical Care Medicine*, vol. 202, no. 5, pp. 681–689, 2020 Sep 1.
- [17] C. Ding, Z. Song, A. Shen, T. Chen, and A. Zhang, "Small molecules targeting the innate immune cGAS–STING–TBK1 signaling pathway," *Acta Pharmaceutica Sinica B*, vol. 10, no. 12, pp. 2272–2298, 2020 Dec.
- [18] M. Hairer and É. Pardoux, "Fluctuations around a homogenised semilinear random PDE," *Archive for Rational Mechanics and Analysis*, vol. 239, no. 1, pp. 151–217, 2021.
- [19] X. L. Sun, R. Ashok, Q. Q. Gao et al., "[PDE-5i combined with RigiScan-based audiovisual sexual stimulation test versus nocturnal penile tumescence test in evaluation of erectile function]," *Zhonghua Nan ke Xue*, vol. 26, no. 7, pp. 601–604, 2020 Jul.